Iranian Journal of Science and Technology, Transactions of Civil Engineering
https://doi.org/10.1007/s40996-024-01675-4

RESEARCH PAPER

Experimental Evaluation of Brick Unreinforced Masonry Wall Out-of-Plane Capacity and Modeling Using the Yield Line Method

Fernando A. Osorio[1,2] · Jose F. Baena[1,3] · Juan D. Jaramillo[1] · Ana B. Acevedo[1]

Received: 19 July 2022 / Accepted: 7 November 2024

Abstract
This paper presents a theoretical model to estimate the out-of-plane (OOP) force capacity of brick unreinforced masonry (URM) walls with strong units and weak joints by applying virtual work and yield line theories for homogeneous plates. The OOP force capacity of the wall was assessed by considering mechanical properties, support conditions, external axial load, and self-weight load. The ultimate vertical and horizontal moments were calculated according to displacement and force models, respectively, developed in previous works. These models consider wall and brick geometry, shear and compression stresses in the joint–brick interface, and support conditions of the wall. The theoretical model presented herein combines the previous models while adding the tensile strength (f_{mt}) of the mortar and assuming elastoplastic behavior of the ultimate moments in both directions. The proposed model constitutes a useful tool to assess the OOP force capacity of brick URM walls with one-way and two-way bending configurations. This paper presents results from experimental shaking table tests and test results from previously published works to validate the proposed model. The comparison between experimental and theoretical results revealed that the developed model predicts the OOP capacity if the appropriate information is available.

Keywords Out-of-plane force capacity · Brick unreinforced masonry walls · Virtual work theory · Yield lines theory

1 Introduction

Unreinforced masonry (URM) structures are recognized as one type of construction most vulnerable to earthquakes (Bruneau 1994; Salgado-Gálvez et al. 2013). Out-of-plane (OOP) vulnerability of URM walls is a central aspect of this problem since OOP failures have been widely reported after seismic events by several research projects and remain one of the causes of collapse and severe damage in buildings (e.g., D'Ayala and Paganoni 2011; D'Ayala and Speranza 2003; Decanini et al. 2004; Giuffrè, 1994; Moon et al. 2014; Oyarzo-Vera and Griffith 2009; Page 1991; Penna et al. 2014). During an earthquake, URM walls resist gravity and shear forces. The in-plane capacity of walls resists shear force, but they must also resist OOP acceleration, which earthquakes impose on their mass. OOP capacity is provided by bending around the "x" and "y" axes, corresponding to the direction of length and height of the wall, respectively. The bending capacity obeys mechanisms that depend on the support conditions of the wall. Figure 1 shows the configuration of bricks on a typical URM wall and the principal directions of analysis ("x" and "y"), which are also the directions of the ultimate vertical and horizontal moments, M_{Rx} and M_{Ry}, respectively.

Several researchers have performed experimental tests and have developed theoretical models to assess the ultimate vertical moment of URM walls subjected to OOP acceleration, M_{Rx}, (Doherty et al. 2002; Penner and Elwood 2016a; Sorrentino et al. 2008; Tomassetti et al. 2018) and the OOP capacity when vertical and horizontal bending capacity are activated (Derakhshan et al. 2018; Graziotti et al. 2019; Griffith et al. 2007a, b; Griffith and Vaculik 2007; Jaramillo et al. 2008; Messali et al. 2017; Sharma et al. 2020a, b; Vaculik and Griffith 2017, 2018). These studies have led to important achievements, but at times diverge (Sorrentino et al. 2017).

✉ Fernando A. Osorio
fosorio@eafit.edu.co

[1] Escuela de Ingeniería, Universidad EAFIT, Carrera 49, Número 7 Sur 50, Medellín, Antioquia, Colombia

[2] Grupo Química Básica, Aplicada y Ambiente–ALQUIMIA, Facultad de Ciencias Exactas y Aplicadas, Instituto Tecnológico Metropolitano, Calle 73, número 76A-354, Medellín, Antioquia, Colombia

[3] Université Catholique de Louvain, Place de L'Université 1, 1348 Ottignies-Louvain-la-Neuve, Leuven, Belgium

Published online: 12 December 2024

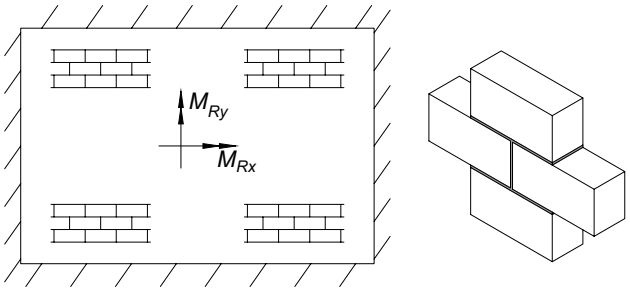

Fig. 1 Brick configuration and direction of resistant moments in a URM wall

Regarding the estimation of the capacity of URM walls to withstand OOP forces through M_{Rx}, Doherty et al. (2002) propose a displacement-based model using a trilinear force–displacement relationship. The authors highlighted that the proposed model presents a better representation for walls subjected to high accelerations and low displacements. On the other hand, Penner and Elwood, (2016a, b) conducted shake table tests on five full-scale URM specimens, considering the flexibility of the diaphragms to which the walls are usually connected at their lower and upper edges. With the results of these tests, they validated a model (Penner and Elwood 2016b) capable of predicting the seismic intensity that causes the collapse of URM walls subjected to the conditions set in the tests conducted. Tomassetti et al. (2018) presented an SDOF model to predict the displacement and force capacity of single-leaf and cavity URM walls subjected to OOP forces, calibrated using results from experimental shake table tests.

For the estimation of the capacity of URM walls to withstand OOP forces through M_{Rx} and M_{Ry}, several works stand out, including those by Griffith and Vaculik (2007), Vaculik and Griffith (2017), Graziotti et al. (2019), and Sharma et al. (2020a, b). Griffith and Vaculik (2007) conducted pseudo-static tests on eight full-scale URM walls, including six with windows, applying OOP pressure to the walls using air bags. They discovered a certain ductility in the walls under this loading condition, with a consequent displacement capacity after reaching their maximum force-bearing capacity. The test results were compared with the predictions obtained by the authors using mathematical expressions based on virtual work, showing agreement between the two types of results. Vaculik and Griffith (2017) developed a nonlinear inelastic displacement-based model to represent the behavior of URM walls subjected to OOP forces without considering tensile strength in the wall joints and assuming they are cracked. The model results were compared with those obtained from previous experiments (Griffith et al. 2007a, b; Vaculik et al. 2004), showing a conservative estimate of the walls' capacity to withstand OOP forces. Graziotti et al. (2019) presented the results of subjecting three single-leaf URM walls (one of them with a window) and a cavity wall to OOP forces using a shake table. The authors highlighted the influence of torsional shear resistance of the bed joints on the walls' capacity to withstand OOP forces and mentioned the capability of the model proposed by Griffith and Vaculik (2007) to predict the capacity of URM walls to withstand OOP forces. Finally, Sharma et al. (2020a, b) presented the results of subjecting four URM specimens to OOP forces on a shake table. One of these four specimens was also subjected to vertical accelerations. The authors aimed to develop strong unit-weak joint (SU_WJ) walls; however, the results showed behavior contrary to this goal, attributing this to an underestimation of the torsional shear resistance developed in the bed joints.

The model developed herein combines the yield line (YL) method with virtual work to estimate the OOP force capacity of brick URM walls. M_{Rx} and M_{Ry} are calculated according to Doherty et al. (2002) and equations developed by Jaramillo (2002) and later modified by Jaramillo et al. (2008), respectively. Tensile strength (f_{mt}) is included in the equations used to calculate M_{Rx} and M_{Ry}. Support conditions, mechanical properties of masonry and individual materials, and brick and joint geometry are considered in the model development. The considered mechanical properties include tensile strength, cohesion, and coefficient of friction in the brick–mortar interface of the bed joints, elasticity modulus of bricks, masonry specific weight, and elasticity and shear modulus of the mortar.

Seven shaking table tests were performed at the Seismic Engineering Laboratory of EAFIT University to validate the theoretical model. Tests were conducted to evaluate the influence of two variables: mortar strength properties (compression and tensile strength) and support conditions. Experimental results from this study and those from other published works are compared to estimations from the analytical model presented in this work.

It must be mentioned that despite the significant impact of the interaction between in-plane and OOP forces acting on brick URM walls on their bearing capacity (Najafgholipour et al. 2013, 2014), this interaction has not been considered in this work.

This paper is divided into four sections. After a brief introduction in the first section, the theoretical YL and virtual work model, including equations from Doherty et al. (2002) and Jaramillo et al. (2008), are described in Sect. 2. Material characterization tests, test setup, and the primary experimental results are presented in Sect. 3. Comparisons between experimental results, prediction of the theoretical model, and experimental work from other research teams have been included in Sect. 3. Finally, the last section contains the conclusion and discussion of the study.

2 Theoretical Model

In this section, YL theory and virtual work are briefly explained. The ultimate resistant moments in the principal wall directions and their combination in the diagonal resistant moment (M_{RD}) are described.

2.1 Yield Line Method

The YL method has been widely applied to calculate the bending capacity of concrete slabs. The method predicts the uniformly distributed force perpendicular to the wall plane by considering its support conditions and ultimate resisting moments in the two main directions. The YL method proposes that the maximum uniform load supported by the slab is reached when the moment acting along all YLs is equal to the ultimate moment. In other words, all YLs exhibit elasto-plastic behavior (Darwin et al. 2016).

The rules of the YL method applied to calculate the OOP force capacity of brick URM walls in this work are listed below.

- YLs are straight.
- YLs represent the intersection of two planes.
- YLs represent axes of rotation.
- The supported line edges of the walls are YLs. The bending capacity along these YLs depends on the edge constraint and axial load.
- A YL between two wall segments must pass through the point of intersection of the axes of rotation of the adjacent wall segments.

Following these rules, it is possible to propose a location for the YLs in each of the possible support conditions and length (L) to height (H) ratios of brick URM walls. Figure 2 shows these patterns as defined by values a and b. Section 2.2 establishes the procedure to determine these values. The gray dot appearing on each support condition case is assumed to be the maximum virtual displacement point.

It is worth remarking that the lateral edge support conditions are given by the returning walls, which are usually perpendicular to the wall subjected to OOP forces. It is assumed to be a fixed-type support, where resistant bending capacity is developed, as established in the rules of the YL method. It must be said that the proposed methodology applies to brick URM walls with strong units and weak joints (SU–WJ). According to Sharma et al. (2021) this means that the YLs will preferably border the units and, therefore, diagonal YLs will be staggered.

2.2 Virtual Work

The virtual work method equates the external work (W_e) generated by loads that cause a virtual deflection in the wall, with the internal work (W_i) generated by the ultimate moment along the YL due to the rotation caused by the virtual deflection. W_e and W_i are calculated using Eqs. (1) and (2), respectively:

$$W_e = t\gamma \int_0^L \int_0^H u(x,y)dxdy \tag{1}$$

$$W_i = \sum_{i=1}^{n} M_{Ri} l_i \varphi_i \tag{2}$$

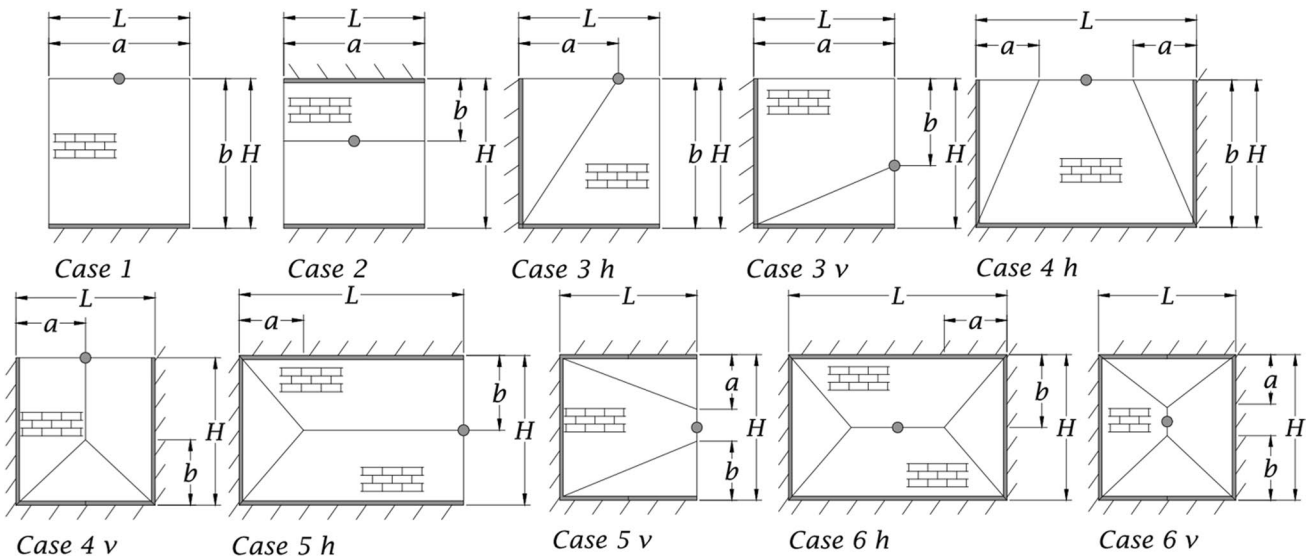

Fig. 2 Support conditions and yield line patterns

where t is the thickness of the wall, γ is the unit weight of the wall; $u(x, y)$ is the displacement of each point of the wall due to virtual deflection, U, which is assumed to occur at the point indicated by a gray dot in each support condition case presented in Fig. 2; L and H are the length and height of the wall; M_{Ri} is the assumed-constant ultimate moment by unit length along YL_i; l_i is the length of YL_i; φ_i is the rotation around YL_i; and n is the number of YLs on the wall surface.

The OOP force capacity is found by choosing the lowest relation between internal and external work using Eq. (3):

$$OOP\ Capacity(g) = min\left(\frac{W_i}{W_e}\right) \tag{3}$$

To find the OOP force capacity of a wall, the following procedure must be done: (*i*) reasonable values for a and b (shown in the YLs patterns in Fig. 2) are proposed; (*ii*) W_e is calculated for a virtual displacement at a point located according to a and b values; (*iii*) W_i is obtained after calculating the M_{Ri}, l_i, and φ_i for each YL as a function of a and b values; (*iv*) the OOP force capacity is calculated using Eq. (3); (*v*) a and b are modified and steps *ii*, *iii,* and *iv* are repeated; (*vi*) the last value of OOP capacity is compared to the previous value and the lowest is kept; (*vii*) steps *v* and *vi* are repeated until the entire wall surface is covered.

2.3 Ultimate Resistant Moments

This subsection explains how the ultimate horizontal, vertical, and diagonal moments are determined. The ultimate vertical and horizontal moments are described using the models proposed by Doherty et al. (2002) and Jaramillo et al. (2008), respectively. A methodology to calculate the ultimate diagonal moment is defined with the previous proposals at diagonal YLs, where both mechanisms are activated.

2.3.1 Ultimate Horizontal Moment, *MRy*

The ultimate horizontal moment, *MRy*, is calculated using the theoretical model proposed by Jaramillo et al. (2008), which is a modification of the original version presented by Jaramillo (2002). This model predicts the ultimate OOP capacity of brick URM walls when only the horizontal capacity mechanism is activated. This model establishes that OOP capacity depends on the capacity of bed joints to resist shear forces and the capacity of head joints to resist tension and compression caused by rotation and displacement between bricks. Figure 3 presents the basic unit configuration of the horizontal bending mechanism, deformations during its activation, and the linear compressive–tensile stress distribution on the head joint.

The flexural acting moment is resisted by shear stresses on the bed joints due to the rotation (θ) illustrated in Fig. 3. According to the elasticity theory model for torsion on a rectangular section (Timoshenko and Goodier 1951), these stresses are distributed on the bed joint. Additionally, the tensile and compressive normal stresses of the head joint contribute to the ultimate horizontal moment (M_{Ry}). An asymmetric linear stress distribution is considered for these stresses, as shown in the right-most illustration in Fig. 3. The tensile area goes until the tensile strength (f_{mt}) of the URM is reached. The asymmetric stress distribution requires a displacement ($\delta = \Delta - j_v$) that occurs at the middle point of the joint, as shown in Fig. 3, and which causes the neutral axis to move towards the compressed area and generate an additional shear stress distribution on the bed joint (considered to be uniform).

To guarantee the equilibrium of axial forces acting on the masonry unit, Eq. (4) (reordered in Eq. (10)) is proposed to represent the relation between δ and θ as a function of mortar elasticity and shear modulus, unit and joints dimensions, and f_{mt} expressed as a fraction (α) of the tensile stress that occur due to the displacement δ.

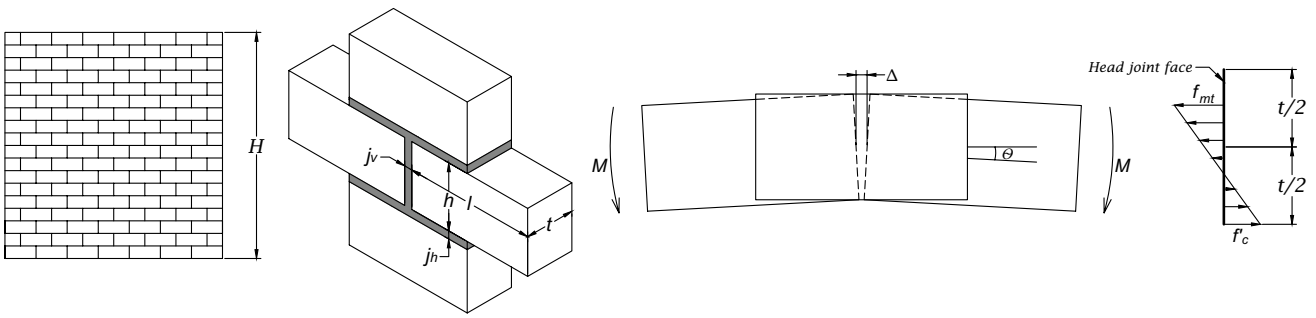

Fig. 3 Basic unit configuration of horizontal flexion mechanism and normal stress distribution on the head joint. Adapted from (Jaramillo et al. 2008)

$$4\eta^2\left(1-\alpha^2\right)-2\eta\left(2+r_G r_m r_b\right)+1=0. \tag{4}$$

To find the URM wall M_{Ry}, an iterative process through Eqs. (4)–(17) must be conducted. An α value is proposed to calculate η using Eq. (10). Then, θ is calculated using Eq. (11). Using the values obtained for η and θ, δ is calculated with Eq. (9). A value for f_{mt} is calculated using Eq. (13) and compared to the URM f_{mt} obtained through characterization tests. If the difference between these two values is insignificant, M_{Ry} can be calculate using Eq. (17). Otherwise, a new value for α must be proposed and all variables recalculated.

$$M_{Ryu}=M_{RT}+M_{RC} \tag{5}$$

$$M_{RT}=\frac{\theta G_M K_T}{j_h} \tag{6}$$

$$K_T=L_M {L_m}^3 k_1 \tag{7}$$

$$M_{RC}=\frac{E_M\theta t^3 h}{12 j_v}\left(4\eta^3(1+\alpha^2(2\alpha-3))-3\eta+1\right) \tag{8}$$

$$\delta=\theta t\eta \tag{9}$$

$$\eta=\frac{2\left(2+r_G r_m r_b\right)\pm\sqrt{\left[2\left(2+r_G r_m r_b\right)\right]^2-16\left(1-\alpha^2\right)}}{8\left(1-\alpha^2\right)} \tag{10}$$

$$\theta=\frac{\tau_{max}2j_h}{t(G_M k+2G_M\eta)} \tag{11}$$

$$\tau_{max}=f_{v0}+\mu\left(\frac{P+Wy}{t}\right) \tag{12}$$

$$f_{mt}=\frac{\delta E_M\alpha}{(j_v/2)} \tag{13}$$

$$k=2\frac{k_1}{k_2} \tag{14}$$

$$k_1=\left[\frac{1}{3}-0.21\frac{L_m}{L_M}\left(1-\frac{{L_m}^4}{12{L_M}^4}\right)\right] \tag{15}$$

$$k_2=\left[3\left[\begin{array}{c}1+0.6095\left(\frac{L_m}{L_M}\right)+0.8865\left(\frac{L_m}{L_M}\right)^2\\-1.8023\left(\frac{L_m}{L_M}\right)^3+0.91\left(\frac{L_m}{L_M}\right)^4\end{array}\right]\right]^{-1} \tag{16}$$

$$M_{Ry}=N\left[\frac{E_M\theta t^3 h}{12 j_v}\left(4\eta^3(1+\alpha^2(2\alpha-3))-3\eta+1\right)+\frac{\theta G_M K_T}{j_h}\right] \tag{17}$$

Variables involved in the M_{Ry} calculations and needed to assess the OOP force capacity of brick URM walls using the herein proposed model are listed and described below.

- H: total height of the wall
- h, l, and t: dimensions of the masonry unit
- j_v and j_h: thickness of the head joint and bed joint, respectively
- θ and δ: angle of rotation and horizontal displacement of the masonry unit, respectively
- M_{RT}: ultimate moment of the basic unit due to torsional and shear stress in the bed joint
- M_{RC}: ultimate moment of the basic unit due to compressive and tensile stress in the head joints
- K_T: torsional stiffness of the bed joint involved in the flexion mechanism (Timoshenko and Goodier 1951)
- L_M and L_m: long and short dimensions, respectively, of the rectangular portion of the bed joint under torsional stresses in the basic unit of the flexion mechanism; depending on brick dimensions, L_M and L_m can take values of t and $(l-j_v)/2$ or vice versa.
- G_M and E_M: shear and elasticity modulus of the mortar, respectively
- τ_{max}: shear strength of the mortar joint–masonry unit interface depending on the cohesion (f_{v0}), friction coefficient (μ), axial load on the wall (P), and the portion of the weight of the wall (Wy) over the bed joint
- η: value that represents the equilibrium of axial forces acting on the masonry unit when the ultimate horizontal moment is reached; Eqs. (4) and (10) consider only the strength contribution of one bed joint of the basic unit of the horizontal flexion mechanism
- α: value that depends on tensile strength of the mortar joint–masonry unit interface, f_{mt}
- r_G: ratio between shear and elasticity modulus of the mortar (G_M/E_M)
- r_m: aspect ratio of the bed joint and head joint (j_v/j_h)
- r_b: aspect ratio of horizontal and vertical faces of the brick in contact with mortar ($(l-j_v)/h$)
- k: coefficient that depends on the geometric section of the mortar subjected to torsion (Timoshenko and Goodier 1951)
- k_1 and k_2: numerical factors that depend on the geometry of the torsional mortar section (Young and Plunkett 2002).
- N: number of bed joints per unit of length throughout the wall height

As can be seen in the equations stablished for the OOP force capacity model, f_{v0} and f_{mt} were considered, which implies a fully fixed bond between the bricks and mortar joints. Other researchers have found that this bond is achieved by bringing the bricks to a saturated-dry surface condition (Maheri et al. 2011).

As established in previous works, torsional shear resistance in bed joints is a paramount parameter to assess the M_{Ry} of brick URM walls (Orduña and Lourenço 2005; Sharma et al. 2021). Further research is needed to improve the model proposed herein to include a better understanding of the coefficients involved in the estimation of shear resistance in bed joints.

2.3.2 Ultimate Vertical Moment, M_{Rx}

The ultimate vertical moment, M_{Rx}, of a brick URM wall depends on several factors: geometry of the wall, axial stress, support conditions of the wall edges, and density of the masonry.

Doherty et al. (2002) proposed a displacement-based methodology to estimate M_{Rx} when the wall presents a horizontal crack at medium height, which divides the wall into two rigid bodies. M_{Rx} is found by stability analysis. The tensile strength of the mortar, f_{mt}, is not considered in the methodology presented by Doherty et al. (2002).

This research proposes calculating M_{Rx} considering f_{mt} and the possibility of a horizontal crack appearing at any point throughout the entire height of the wall. Figure 4 presents the stresses of a URM wall with the specific support condition "*Case 2*" when the ultimate capacity is reached. The horizontal displacement needed at the middle strip of a URM wall to develop f_{mt} at its top or bottom edges is within a range of 0.10–5.00 μ m, depending on the values of f_{mt}, mortar elasticity modulus, and the point where the central crack is formed. Taking this into account and considering that the collapse forces transmitted to the wall during an earthquake are almost

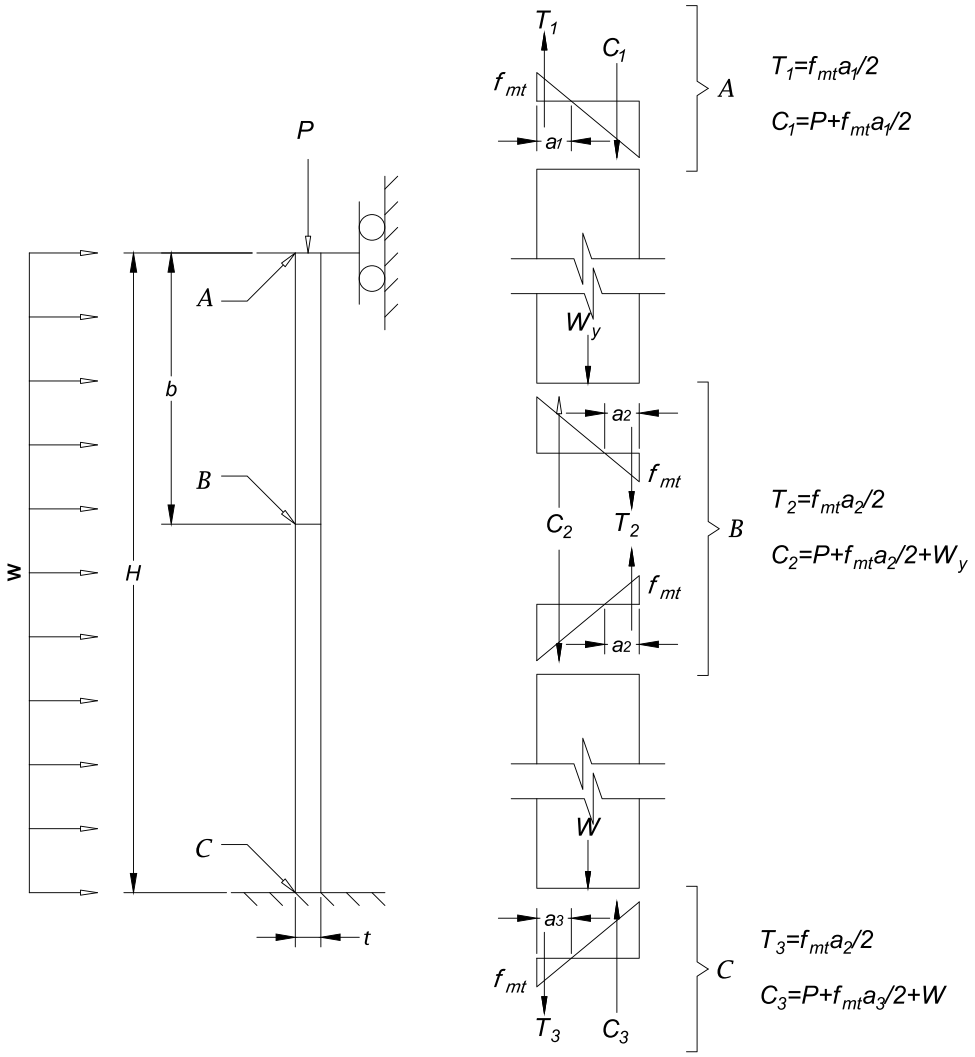

Fig. 4 URM wall stress state under support condition "Case 2"

instantaneous, it is assumed in the model proposed here that f_{mt} is reached at the same time in the three YLs. The authors recognized that there is no experimental evidence of this behavior, but it is a convenient approximation to the reality that considers all variables involved in the problem. It is also valuable to mention that some experiments have shown that a brick URM wall can develop cracks in bed joints before reaching its peak force capacity (e.g. Graziotti et al. 2019; Sharma et al. 2020a, b; Vaculik and Griffith 2018, 2007).

The ultimate horizontal moments presented on the three YLs, with these support conditions, are calculated using Eqs. (18), (19) and (20):

$$M_{RxA} = \frac{1}{6}\left[f_{mt}t^2 + Pt\right], \tag{18}$$

$$M_{RxB} = \frac{1}{6}\left[f_{mt}t^2 + Pt + Wyt\right], \tag{19}$$

$$M_{RxC} = \frac{1}{6}\left[f_{mt}t^2 + Pt + Wt\right], \tag{20}$$

where W is the self–weight per unit of length of the wall and y is the relative height where the horizontal crack appears, calculated as $y = b/H$. The b value is found with the smallest possible internal work, W_i, considering the mechanical and geometrical characteristics of the wall. The abovementioned variables are needed to assess the OOP force capacity of brick URM walls with the model proposed here.

2.3.3 Ultimate Diagonal Moment, M_{RD}

The ultimate diagonal moment, M_{RD}, is calculated by combining the ultimate horizontal moment, M_{Ry}, and the ultimate vertical moment, M_{Rx}, using tensorial transformation. The M_{RD} is calculated with Eq. (21), following the criterion proposed by Griffith and Vaculik (2007), where φ is the angle of the diagonal YL with the horizontal, which depends on the values of a and b. To determine the values of a and b, the masonry unit bonding pattern is considered (see Figs. 1, 6 and 8), with a varying at a rate of $l + j_v$, and b varying at a rate of $h + j_h$ (see Fig. 3) during the iteration for calculating the OOP force capacity of the wall as described in Sect. 2.2. It is assumed, according to the results reported in Griffith and Vaculik (2007), that the two resistant mechanisms are elastoplastic, and both are present at the same time on all diagonal YLs. Since M_{Ry} and M_{Rx} are variable through the height of the wall, M_{RD} is calculated for both end points of the diagonal YL and the average of these two values is used as the ultimate resistant moment of the diagonal YL:

$$M_{RD} = (sen\varphi)^2 M_{Ry} + (cos\varphi)^2 M_{Rx}. \tag{21}$$

2.4 Remarks

It must be considered that the OOP force capacity calculated with Eq. (3) leads to an effective URM wall acceleration (Ea) since the external work (W_e) is calculated over the entire area of the wall. Therefore, the OOP capacity must be compared to accelerations acting all over the wall (effective acceleration) and not those measured at its bottom.

The elastoplastic behavior assumed in Sect. 2.3.3 is justified by the results obtained by Griffith et al. (2007a, b) and Griffith and Vaculik (2007). The authors of those works discovered a significant ductility in URM walls subjected to OOP forces. Hence, if one of the ultimate resistant moments described above is reached before the other during the application of OOP forces, the wall could stand until the other one is reached. However, it should be noted that the load applied in the tests conducted by these authors was of a cyclic/static type, which may have contributed to the ductility observed in the walls.

It is essential to know that the model proposed here should be used to assess the OOP force capacity of SU–WJ brick URM walls since the failure of the wall is assumed to develop not through the masonry units but through the wall joints.

The authors recognize the limitations of the proposed model due to the assumption of reaching f_{mt} at the same time in the three horizontal YLs, as explain in Sect. 2.3.2, as well as that all the YLs reach their ultimate moment at the same time.

3 Experimental Study

Material characterization, primary test setup, the loading procedure, the main results from the experimental study, and a comparison with theoretical model results are provided in this section.

The goals of the experimental study were to validate the proposed model and assess the influence of boundary conditions and f_{mt} of joints in brick URM walls OOP force capacity. Three boundary conditions were applied, and two different f_{mt} mortars were used to build the experimental specimens.

3.1 Material Characterization Tests

To characterize the materials used to build the specimens tested in the experimental study, masonry compression (f'_m) (ASTM-International 2012) and diagonal crack shear strength (f_t) (ASTM-International 2010b), mortar compression strength (f'_{cp}) (ASTM-International 2017) for two different mortar qualities, brick compression strength (f'_u) (ASTM-International 2007), and cohesion (f_{v0}), friction

coefficient (μ), and tensile strength of the joints (f_{mt}) tests were carried out. Table 1 presents the mean values and standard deviation of each test.

f_{mt} was obtained from five specimens constituted of two units and one $f'_{cp1} = 7.18$MPa mortar joint subjected to flexural stresses by applying the ASTM C78 (ASTM-International 2010a) standard. f_{mt} was calculated using Eq. (22):

$$f_{mt} = \frac{3PL}{2t^2 l} \tag{22}$$

where P is the measured applied load, L is the specimen spam, and t and l are the thickness and length of the units, respectively.

The value obtained for μ is lower than expected, but the procedure described in British Standard (BSi) BS EN 1052-3, 2002 (British-Standards 2010) was followed to experimentally assessed it together with f_{v0}. Furthermore, a lower value of μ can be considered a characteristic of weak joints, as it is needed to apply the proposed OOP force capacity assessment methodology.

In Table 1 it can be seen that two f'_{cp} mortars were used. The bond between units of the specimens built using the $f'_{cp2} = 1.04$MPa mortar was broken by hand before the mortar was completely hardened to obtain a zero (0) f_{mt} and, consequently, a zero f_{v0}. This process was done for each unit of each row (understood as the line of units between two bed joints) to evaluate the influence of f_{mt} on the wall OOP force capacity. μ was assumed the same value for both mortar qualities; f'_m is not needed to assess the OOP capacity using the proposed model, so it was not tested for the masonry built using the weak mortar. It was not possible to test f_t for this masonry since it has no cohesion between masonry units and mortar.

3.2 Specimens

Seven specimens were subjected to sinusoidal cyclic loading to measure the influence of two independent variables on OOP capacity: support conditions and mortar quality (f'_{cp} and f_{mt}, respectively).

The specimens represent slender walls found in typical brick URM dwelling constructions in Colombia. Their dimensions were defined according to architectural plans collected during the earlier phase of this project. All specimens were 2.484-m high, 3.25–4.08-m wide, and 0.09-m thick. The specimens were built using standard horizontally hollowed clay bricks with grooved surfaces. Typical bricks were 0.39-m long, 0.19-m high, and 0.09-m thick. Bricks were brought to a saturated-dry surface condition to achieve a fixed bond between the mortar and bricks, following the recommendations given in previous research (Maheri et al. 2011). Bed and head joints were 0.017-m thick, considering that it is not common to find typical 0.01-m-thick joints in Colombian brick URM buildings. Every wall featured 12 rows of bricks. Three support conditions were used, represented by the "*C#*" in each specimen code, and the conditions were correlated to the support condition cases presented in Fig. 2. Whenever the support condition case code has a single quotation mark (') at the end, it means that the specimen had not vertical displacement restriction nor rotational restriction along the upper edge while lateral displacement was avoided. Figure 5 shows schemes for each of the support conditions applied to the specimens. The characteristics of the specimens are summarized in Table 2. From this table, it is easy to identify the meaning of each code portion of the specimen.

3.3 Test Setup

The most important parts of the test setup are identified by numbers in Fig. 6, where two examples of specimens are shown (C5 and C2 support conditions at the left and right, respectively). Test specimens (1) were built directly on the shaking Table (2) at EAFIT University. A steel beam *C*-shaped profile (3) was fixed to the shaking table and filled with concrete to represent a realistic surface at the bottom of the specimens. Stiff steel frames (4) were used to support a second steel beam (5), which was filled with concrete to impose the top support conditions. Stiff steel frames were also built to ensure that the top and bottom edges of the specimens moved without relative displacement between them. Therefore, the acceleration in both points was identical. Accelerometers were placed at the base (6) and mid-height (7) of each specimen.

Additionally, a linear variable differential transformer (LVDT) (8) was located close to the mid-height accelerometer. The accelerometer at the base of the specimen was maintained for the entire test, but the LVDT and accelerometer at the middle height of the specimen were removed after

Table 1 Results of material characterization tests

	f_t(MPa)	f'_m(MPa)	f'_{cp1}(MPa)	f'_{cp2}(MPa)	f_{mt}(MPa)	f'_u(MPa)	f_{v0}(MPa)	μ
Mean	0.63	1.93	7.18	1.04	0.16	2.74	0.29	0.25
Standard deviation	0.14	0.30	3.52	0.15	0.01	0.70	0.08	0.26
Number of specimens	9	5	12	6	5	29	9	9

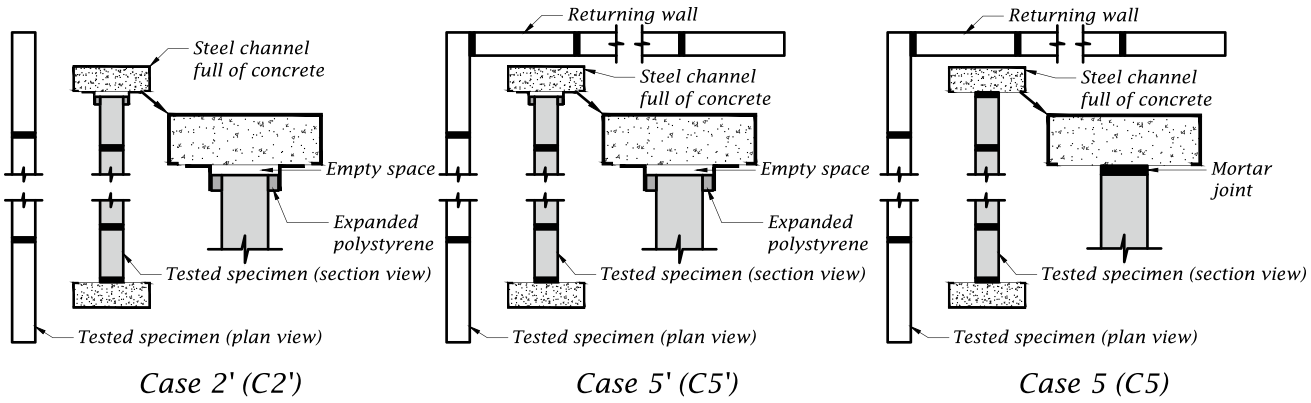

Fig. 5 Support condition schemes

Table 2 Specimen characteristics

Test	Length (m)	Height (m)	Thickness (m)	Support condition	f'_{cp}(MPa)	f_{mt}(MPa)
1-C5-7-328	3.28	2.484	0.09	Case 5	7.18	0.16
2-C5-7-408	4.08			Case 5	7.18	0.16
3-C5'-7-328	3.28			Case 5'	7.18	0.16
4-C5'-7-408	4.08			Case 5'	7.18	0.16
5-C2'-7-325	3.25			Case 2'	7.18	0.16
6-C2'-1-325	3.25			Case 2'	1.04	0.00
7-C5'-1-408	4.08			Case 5'	1.04	0.00

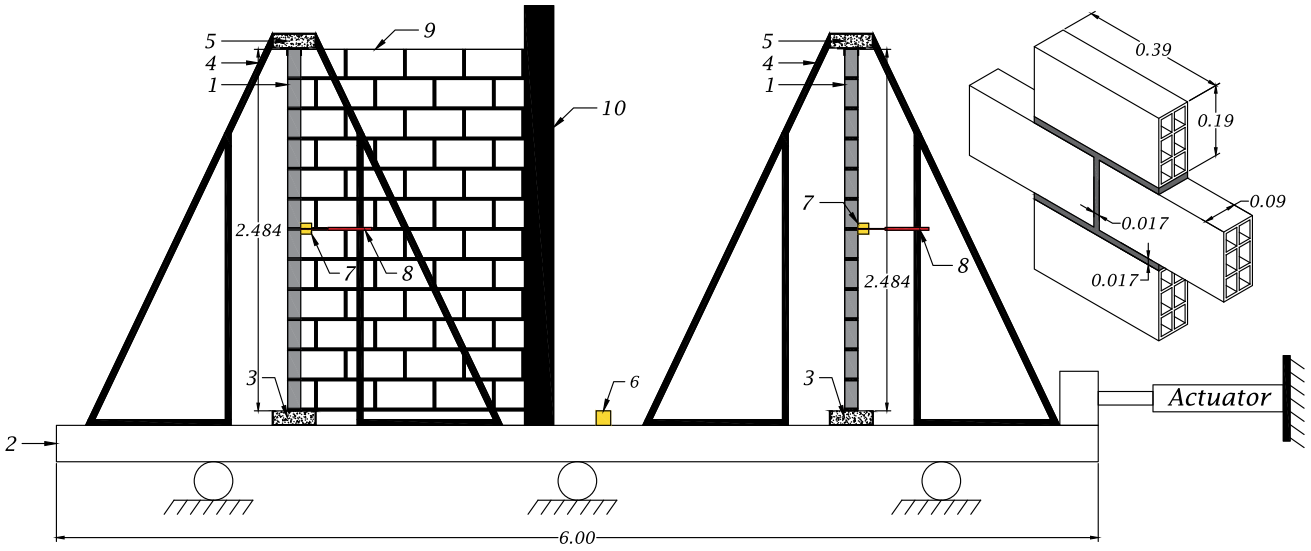

Fig. 6 Test setup

prudent acceleration to preserve the equipment. To achieve the C5 support condition, a transversal brick URM wall (9) was built on one of the vertical edges of the specimen, interlocking the bricks of the returning walls with those of the specimens. The opposite vertical edge of the returning brick URM wall was fixed to a steel beam *C*-shaped profile full of concrete (10) to prevent the wall from moving in the acting force direction.

3.4 Loading Procedure

The specimens were subjected to incremental sinusoidal accelerations in several stages with a frequency close to that of the whole system (the shaking table and test specimen). Incremental sinusoidal acceleration was used to better control the final acceleration carried by the specimens. It also allows higher *Ea* in the shaking table with the same actuator by resonance effects. An example of the incremental sinusoidal records used as input for the test of specimen 7-C5'-1–408 are shown in Fig. 7.

3.5 Experimental and Theoretical Results

The fully detailed experimental results are reported in (Baena-Urrea 2019). This section describes the most relevant test results and the influence of support conditions and mortar quality on OOP force capacity. Table 3 presents obtained experimental and theoretical *Ea* values. The experimental *Ea* value was obtained by multiplying the peak table acceleration of the last stage by the amplification factor presented in Table 3. This factor was calculated by dividing the acceleration at the base and at mid-height before removing the mid-height accelerometer.

Due to this procedure, there can be a non-quantified uncertainty in the experimental *Ea* values reported in Table 3. Ratios of the theoretical and experimental *Ea* are also shown in Table 3, except for specimens 1-C5-7-328, 2-C5-7-408, and 3-C5'-7-328 since they did not collapse during the tests.

Table 3 Summary of test results

Specimen	Experimental *Ea* (g)	Multiplying factor	Theoretical *Ea* (g)	Theo. *Ea* to Exp. *Ea* ratio
1-C5-7-328	1.13*	1.19	1.79	–
2-C5-7-408	1.13*	1.19	1.53	–
3-C5'-7-328	1.25*	1.19	1.49	–
4-C5'-7-408	1.24	1.18	1.25	1.01
5-C2'-7-325	0.89	1.00	0.57	0.64
6-C2'-1-325	0.18	1.00	0.08	0.42
7-C5'-1-408	0.47	1.20	0.45	0.97

*Specimen did not collapse. The shaking table reached its capacity

Specimens 1-C5-7-328 and 2-C5-7-408 represented inter-story walls confined by two slabs at their top and bottom edges. These specimens did not present visible damage or cracks during any of the testing stages, even when exposed to an *Ea* of 1.13 g. Their OOP force capacity was higher than the capacity of the shaking table to impose accelerations. Consequently, the specimens did not

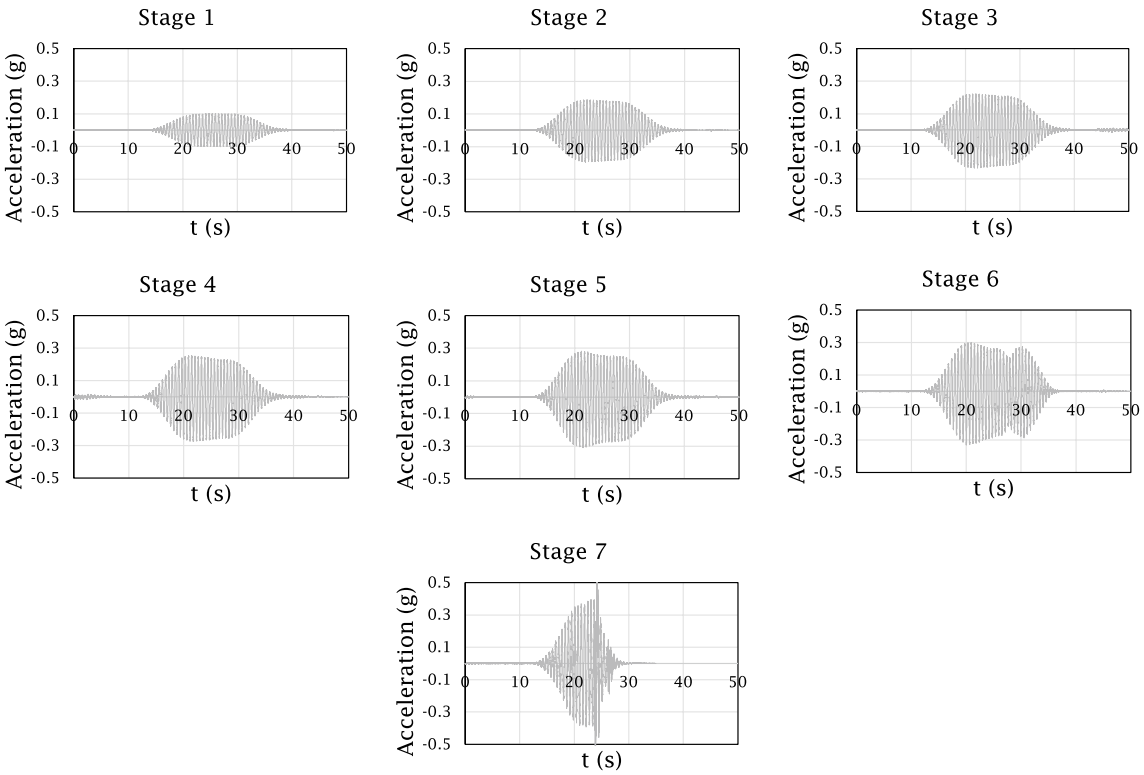

Fig. 7 Incremental sinusoidal accelerations used as input in 7-C5'-1-408 specimen test

collapse. The final states of both specimens are presented in Fig. 8 (A) and (B).

Specimen 3-C5'-7-328 was identical to specimen 1-C5-7-328, but the vertical displacement and rotation at the top edge were released, restricting it to lateral displacement. After being exposed to an *Ea* of 1.25 g, the specimen did not present any visible damage or cracks, as shown in Fig. 8 (C). Once again, the capacity of the shaking table was reached before the collapse of the specimen. That specimen became specimen 5-C2'-7-325 by removing the returning wall at the lateral edge. Finally, the specimen failed at an *Ea* of 0.89 g with a horizontal crack at an approximate height of 1.60 m ($b = 0.884$m), which was visible two load cycles before the specimen collapse (see Fig. 8E). The expected *b* value from the theoretical results was 0.96 m.

Similarly, specimen 4-C5'-7-408 was identical to specimen 2-C5-7-408, but the vertical displacement and rotation at the top edge were released, restricting to lateral displacement. The ultimate *Ea* carried by specimen 4-C5'-7-408 was 1.24 g. The failure took place five cycles after the first crack appeared (horizontal crack), just after the specimen detached from the transverse wall, as shown in Fig. 8D. The bricks of the transverse wall reached their tensile strength and failed due to the imposed acceleration. This means that the specimen had weak units – strong joints (as described by Sharma et al. 2021) in its union with the returning wall, perhaps due to the variability in mortar or unit properties. The specimen collapsed after this failure, exhibiting a horizontal crack at a height 1.60-m from the base ($b = 0.884$m). Figure 8D shows the precise moment of failure from a diagonal view to observe its complete pattern. The expected *b* value from the theoretical results was 1.20 m.

To evaluate the influence of the mortar quality, the last two specimens were built using a poor cement mortar with a compression strength of 1.04 MPa. The bond between units of the specimens built using this mortar was broken before the mortar was completely hardened to obtain zero (0) f_{mt} and, consequently, zero f_{v0}. The *Ea* that specimen 6-C2'-1-325 carried was 0.18 g; it presented a horizontal crack at a height of 1.80 m ($b = 0.684$ m) just before collapsing (see Fig. 8F). A *b* value equal to 0.50-m was obtained from the theoretical results. Additionally, specimen 7-C5'-1-408 resisted an *Ea* of 0.47 g and presented horizontal and diagonal cracks that appeared four cycles before specimen collapse, which indicates that the side edge support was strong enough to activate the horizontal

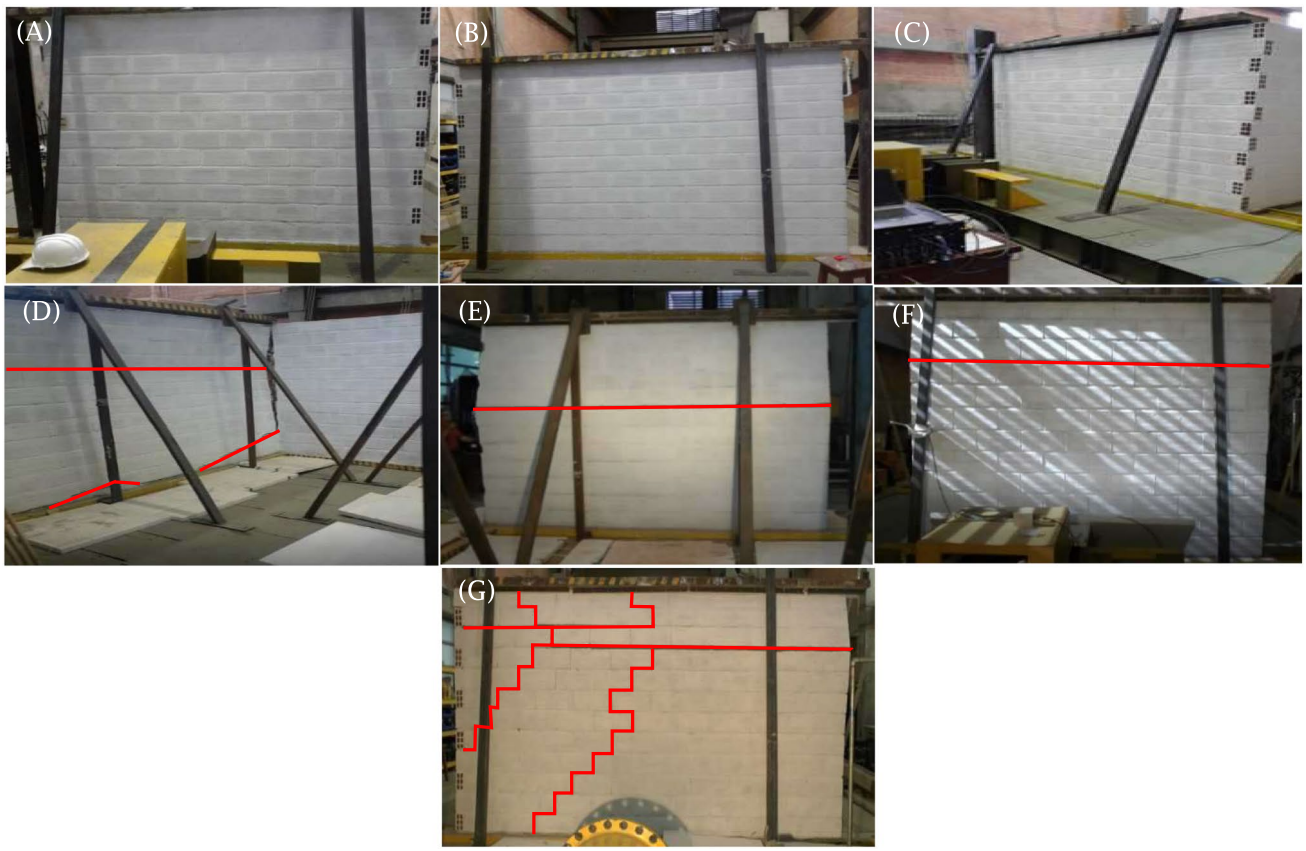

Fig. 8 Final state of unit tests for specimen **A** 1-C5-7-328, **B** 2-C5-7-408, **C** 3-C5'-7-328, **D** 4-C5'-7-408, **E** 5-C2'-7-325, **F** 6-C2'-1-325, and **G** 7-C5'-1-408

bending resistant moment and develop some ductility (see Fig. 8G). The expected *a* and *b* values from the theoretical results were 1.80 m and 0.20 m, respectively, but the experimentally obtained values were 1.20 m and 0.60 m, respectively.

These results show that the quality of the mortar and, thus, f_{mt} has a considerable influence on OOP force capacity. The *Ea* resisted by specimens built with the strong mortar was at least 2.6 times higher than that for specimens built with the weak mortar (comparing specimens 4-C5'-7-408 and 7-C5'-1-408). Table 3 shows that the *Ea* carried by specimen 5-C2'-7-325 was almost five times greater than that of specimen 6-C2'-1-325. Moreover, the specimens with strong mortar were stiffer, which allowed them to resist a greater *Ea* with an equivalent lateral deformation. In Fig. 9, acceleration versus displacement at the initial stages at medium height for all the specimens but one are plotted. Unfortunately, during the first stage of testing of specimen 5-C2'-7-325, the data acquisition system failed. Therefore, accelerometer and LVDT information for this specimen is not available for the first stage.

Additionally, when the walls are vertically confined, i.e., vertical displacement and rotation at the top edge are restricted, the OOP force capacity increases because there is a non-quantified additional reaction at the top edge of the specimen that causes an increase in its stiffness, as shown in Fig. 9B and C. As mentioned above, the failure of the vertically confined specimens (1-C5-7-328 and 2-C5-7-408) could not be reached due to the capacity of the shaking table.

The results also exhibit the influence of the lateral edge support condition on the OOP capacity of the specimens and their failure pattern. The OOP capacity of brick URM specimens supported at bottom and top edges is independent of their length. The results indicate that the lateral support condition significantly increases the ultimate capacity, even for long walls where this support condition is less relevant. The ultimate capacities of specimens 7-C5'-1-408 and 4-C5'-7-408 were 2.6 and 1.4 times higher than 6-C2'-1-325 and 5-C2'-7-325, respectively, but side edge support did not significantly increase the stiffness of the specimens, as shown in Fig. 9D.

It is worth noting that the experimental to theoretical *Ea* ratios for specimens 4-C5'-7-408 and 7-C5'-1-408 presented in Table 3 are very close to one (1.00), while for specimens 5-C2'-7-325 and 6-C2'-1-325, the theoretical values are close to half of those of the experimental. The latter results may be caused by the development of a rotation restriction in the top edges of the specimens, which was assumed to be nonexistent.

3.6 Comparison of Model Results to Experimental Results from Third Parties

The model proposed herein calculates OOP force capacity in terms of *Ea*. Only previous experimental results present as *Ea* carried by the specimens, or any value that allowed to calculate it, were considered. These results were compared with theoretical results obtained by the authors of this work. Additionally, only specimens reported by authors as SU–WJ masonry, or those for which this characteristic was identifiable in the failure crack patterns, were included in this work. In Table 4, experimental results from previously published work that fulfill the above statements are presented. The theoretical *Ea* calculated via the model proposed here, using the material characterization explicitly reported in those reports as input, are also presented in Table 4.

Some significant differences between experimental *Ea* reported by other authors and theoretical *Ea* calculated here can be observed in Table 4. It is important to consider that it was not possible to access some characteristics of the URM used in previous works needed to calculate theoretical *Ea*. In Table 5, missing characteristics and assumed values are presented for each specimen tested in other works. The specimens reported in Table 4 are included in this work since the authors consider it important to have third-party experimental results to validate the proposed model, even though not all specimen mechanical properties were reported in the works from which these data were obtained.

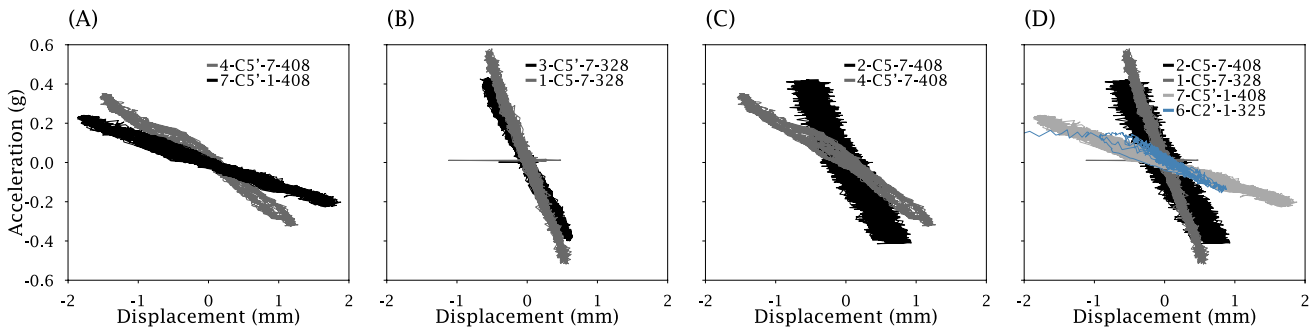

Fig. 9 Displacement vs. acceleration at mid-height

Table 4 Experimental and theoretical results for previously published work

Reference–Specimen	Support condition case	Length (m)–height (m)	Experimental *Ea* (g)	Theoretical *Ea* (g)	Theo. *Ea* to Exp. *Ea* ratio
Dazio (2008)–W2SS	C2’	1.20–2.40	0.18	0.30	1.65
Dazio (2008)–W2CP2	C2’	1.20–2.40	1.20	1.24	1.03
Simsir et al. (2004)–S3	C2’	1.30–1.93	2.04	1.85	0.91
Graziotti et al. (2019)–CS-005-RR	C6	3.98–2.75	2.01	2.44	1.21
Graziotti et al. (2019)–CS-000-RF	C4	3.98–2.75	1.44	1.17	0.82
Graziotti et al. (2019)–CL-000-RF	C4	4.02–2.76	1.71	1.23	0.72
Derakhshan et al. (2018)–B1	C6	4.05–2.53	0.70	0.72	1.04
Vaculik and Griffith (2018)–D1	C6’	1.84–1.23	3.25	5.39	1.66
Vaculik and Griffith (2018)–D2	C6’	1.84–1.23	1.47	2.90	1.97
Griffith et al. (2007a, b)–Wall 1	C6’	4.00–2.50	2.64	3.30	1.25
Griffith et al., (2007a, b)–Wall 2	C6’	4.00–2.50	1.69	1.71	1.01

Table 5 Assumed URM characteristics from other works

Reference–Specimen	Assumed characteristic	Value
Dazio (2008)–W2SS Dazio (2008)–W2CP2	G_M	2500 MPa
	E_M	6250 MPa
	f_{v0}	0.20 MPa
	μ	0.50
Simsir et al. (2004)–S3	G_M	3500 MPa
	E_M	8750 MPa
	f_{v0}	0.20 MPa
	μ	0.50
	f_{mt}	0.05 MPa
Derakhshan et al. (2018)–B1	E_M	52,700 MPa
	f_{v0}	0.13 MPa
	μ	0.50
Vaculik and Griffith (2018)–D1 Vaculik and Griffith (2018)–D2	f_{v0}	0.13 MPa
Griffith et al. (2007a, b)–Wall 1 Griffith et al. (2007a, b)–Wall 2	f_{v0}	0.13 MPa
	μ	0.50
	γ	18.00 kN/m^3

Despite the abovementioned missing data for third-party tests, seven out of eleven experimental *Ea* to theoretical *Ea* ratios are between 0.75 and 1.25, which are considered good results by the authors of this work. Furthermore, ratios obtained for specimens 4-C5’-7-408 and 7-C5’-1-408, give the authors confidence in the proposed model since the input parameters for the theoretical *Ea* were assessed under their supervision.

Despite specimens (Dazio 2008)–W2SS, (Dazio 2008)–W2CP2, and (Simsir et al. 2004)–S3 having a C2’ support condition case, they validate the assumption mentioned in Sect. 2.3.2 and verify the influence of f_{mt} on the OOP force capacity of URM walls.

4 Discussions and Conclusions

A mathematical model to assess the OOP force capacity of brick URM walls and an experimental study to verify the accuracy of the model were presented in this paper. The model combines the equations provided by Jaramillo et al. (2008) and Doherty et al. (2002) with YL and virtual work theories. f_{mt} was included in the calculations of M_{Rx} and M_{Ry}. In the proposed model, it was assumed that walls, under support conditions that allow them to develop both of resistant moments, have certain ductility since the walls will stand until both of resistant moments are reached. This ductility was supported by observations made during the experimental study for specimens 4-C5’-7-408 and 7-C5’-1-408. For these specimens, the theoretical *Ea* to experimental *Ea* ratios were 1.01 and 0.97, respectively. Despite the proposed model assuming applicability only for SU–WJ brick URM walls, the theoretical *Ea* to experimental *Ea* ratio obtained for specimen 4-C5’-7-408, which presented a tensile rupture of the returning wall units, was very close to 1.0. This result indicates that either the failure in the joints of the returning wall and specimen union was almost reached, or there was a weak unit in the returning wall that led to a general tensile failure across the edge.

On the other hand, theoretical results for specimens 5-C2’-7-325 and 6-C2’-1-325 were not close to the experimentally obtained values. The authors attribute this to two different factors: (*i*) there is still work to do in order to improve the proposed model and better assess the influence of f_{mt} on brick URM walls OOP force capacity and (*ii*) the support condition of these two specimens was assumed to develop zero (0) restrictions to rotate at the top edge of the specimen, however, some non-quantified restriction may have occurred.

The ratios between theoretical and experimental results for tests reported in literature show significant dispersion.

The authors of this work attribute it to the lack of important input information to assess the theoretical *Ea* value via the proposed model, since not all the parameters needed for its execution were presented in previously published works developed by other authors. Those parameters were assumed herein by considering an extensive literature review. However, seven of the eleven ratios obtained were close to one. These results provide confidence in the model proposed here.

Regarding the experimental results, it can be seen that (*i*) specimens with the possibility of rotation and vertical displacement at their top edge have a significantly lower OOP force capacity compared with those that do not have this possibility. (*ii*) The OOP force capacity of the brick URM walls increases with the increase of f'_{cp} and f_{mt}. (*iii*) The lateral support condition increases the OOP force capacity of brick URM walls, even in long OOP-loaded walls. (*iv*) This condition also increases wall ductility since it allows development of both M_{Rx} and M_{Ry} under SU–WJ configuration, otherwise a fragile failure may occur.

There is still experimental work needed to better understand the behavior of brick URM walls when subjected to OOP forces and to continue improving the proposed model. However, URM is a very heterogeneous material, and it is difficult to control its mechanical properties.

Acknowledgements The authors want to express their sincere gratitude to the Metropolitan Area of the Aburra Valley (AMVA, Colombia) (https://www.metropol.gov.co/) who financed this project in company with EAFIT University (Colombia) (https://www.eafit.edu.co/) framed in contract number 583 of 2017. The authors acknowledge to BUILD CHANGE Foundation (https://buildchange.org/) for all their support, information provided and their help during the whole experimental program. The authors acknowledge Ladrillera San Cristobal (https://ladrillerasancristobal.com/) for supplying all the bricks needed to build the specimens.

Author Contributions F. Osorio, J. Baena: investigation, data curation, writing—original draft. J. Jaramillo: investigation, supervision, formal analysis. A. Acevedo: funding acquisition, supervision.

Funding This work was financially supported by Metropolitan Area of the Aburra Valley (AMVA, Colombia) and EAFIT University (Colombia) [grant number 583 of 2017].

Declarations

Conflict of interests The authors declare that they have no known competing financial interests or personal relationships that could have appeared to influence the work reported in this paper.

References

ASTM-International (2007) ASTM C67 Standard test methods for sampling and testing brick and structural clay tile

ASTM-International (2010a) ASTM C78 Standard test method for flexural strength of concrete (using simple beam with third-point loading)

ASTM-International (2010b) ASTM E519 Standard test method for diagonal tension (shear) in masonry assemblages

ASTM-International (2012) ASTM C1314-21 Standard test method for compressive strength of masonry prisms

ASTM-International (2017) ASTM C39 Standard test method for compressive strength of cylindrical concrete specimens

Baena-Urrea J (2019) Evaluación experimental de la respuesta fuera del plano de muros de mampostería, no reforzada y reforzada con franjas de mallas electrosoldadas y mortero. Universidad EAFIT

British-Standards (2010) British Standards (BSi) BS EN 1052-3 Methods of test for masonry—part 3: Determination of initial shear strength

Bruneau M (1994) State of the art report on seismic performance of unreinforced masonry buildings. 120(1):230–251

Darwin D, Dolan C, Wilson A (2016) Design of concrete structures (15th ed). McGraw-Hill Education

D'Ayala D, Paganoni S (2011) Assessment and analysis of damage in L'Aquila historic city centre after 6th April 2009. Bull Earthq Eng 9(1):81–104

D'Ayala D, Speranza E (2003) Definition of collapse mechanisms and seismic vulnerability of historic masonry buildings. Earthq Spectra 19(3):479–509

Dazio A (2008) The effect of the boundary conditions on the out-of-plane behaviour of unreinforced masonry walls. In: Proceedings of the 14th world conference on earthquake engineering

Decanini L, de Sortis A, Goretti A, Langenbach R, Mollaioli F, Rasulo A (2004) Performance of masonry buildings during the 2002 Molise, Italy, earthquake. Earthq Spectra 20(S1):S191–S220

Derakhshan H, Lucas W, Visintin P, Griffith M (2018) Out-of-plane strength of existing two-way spanning solid and cavity unreinforced masonry walls. Structures 13:88–101

Doherty K, Griffith M, Lam N, Wilson J (2002) Displacement-based seismic analysis for out-of-plane bending of unreinforced masonry walls. Earthq Eng Struct Dyn 31(4):833–850

Giuffrè A (1994) Seismic safety and strengthening of historical buildings and urban fabrics. In: Proceedings of the 10th world conference on earthquake engineering, vol 11, pp 6583–6596

Graziotti F, Tomassetti U, Sharma S, Grottoli L, Magenes G (2019) Experimental response of URM single leaf and cavity walls in out-of-plane two-way bending generated by seismic excitation. Constr Build Mater 195:650–670

Griffith M, Vaculik J, Lam N, Wilson J, Lumantarna E (2007a) Cyclic testing of unreinforced masonry walls in two-way bending. Earthq Eng Struct Dyn 36(6):801–821. https://doi.org/10.1002/eqe.654

Griffith M, Vaculik J (2007) Out-of-plane flexural strength of unreinforced clay brick masonry walls. TMS J 25(1):53–68

Griffith M, Vaculik J, Lam N, Wilson J, Lumantarna E (2007b) Cyclic testing of unreinforced masonry walls in two-way bending. Earthq Eng Struct Dynam 36(6):801–821

Jaramillo J (2002) Mecanismo de transmisión de cargas perpendiculares al plano del muro en muros de mampostería no reforzada. Revista De Ingeniería Sísmica 67:53–78

Jaramillo J, Morales M, Hincapié G (2008) Respuesta sísmica de muros de mampostería no reforzada sometidos a aceleraciones perpendiculares a su plano. Revista Internacional De Desastres Naturales, Accidentes e Infraestructura Civil 8(2):183–200

Maheri MR, Motielahi F, Najafgholipour MA (2011) The effects of pre and post construction moisture condition on the in-plane and out-of-plane strengths of brick walls. Mater Struct/Materiaux et Construct 44(2). https://doi.org/10.1617/s11527-010-9648-y

Messali F, Ravenshorst G, Esposito R, Rots J (2017) Large-scale testing program for the seismic characterization of Dutch masonry walls.

In: Proceedings of the 16th European conference on earthquake engineering, 16WCEE, Santiago, CL, 9–13
Moon L, Dizhur D, Senaldi I, Derakhshan H, Griffith M, Magenes G, Ingham J (2014) The demise of the URM building stock in Christchurch during the 2010–2011 Canterbury earthquake sequence. Earthq Spectra 30(1):253–276
Najafgholipour MA, Maheri MR, Lourenço PB (2013) Capacity interaction in brick masonry under simultaneous in-plane and out-of-plane loads. Construct Build Mater 38. https://doi.org/10.1016/j.conbuildmat.2012.08.032
Najafgholipour MA, Maheri MR, Lourenço PB (2014) Definition of interaction curves for the in-plane and out-of-plane capacity in brick masonry walls. Construct Build Mater 55. https://doi.org/10.1016/j.conbuildmat.2014.01.028
Orduña A, Lourenço PB (2005) Three-dimensional limit analysis of rigid blocks assemblages. Part II: Load-path following solution procedure and validation. Int J Solids Struct 42:18–19. https://doi.org/10.1016/j.ijsolstr.2005.02.011
Oyarzo-Vera C, Griffith M (2009) The Mw 6.3 Abruzzo (Italy) earthquake of April 6th 2009: on site observations. Bull New Zealand Soc Earthq Eng 42(4):302–307
Page A (1991) Newcastle earthquake behavior of masonry structures. Masonry Int 5(1):11–18
Penna A, Morandi P, Rota M, Manzini C, da Porto F, Magenes G (2014) Performance of masonry buildings during the Emilia 2012 earthquake. Bull Earthq Eng 12(5):2255–2273
Penner O, Elwood K (2016a) Out-of-plane dynamic stability of unreinforced masonry walls in one-way bending: shake table testing. Earthq Spectra 32(3):1675–1697
Penner O, Elwood KJ (2016b) Out-of-plane dynamic stability of unreinforced masonry walls in one-way bending: Parametric study and assessment guidelines. Earthq Spectra 32(3). https://doi.org/10.1193/011715EQS011M
Salgado-Gálvez M, Zuloaga-Romero D, Bernal G, Mora M, Cardona O-D (2013) Fully probabilistic seismic risk assessment considering local site effects for the portfolio of buildings in Medellín, Colombia. Bull Earthq Eng https://doi.org/10.1007/s10518-013-9550-4
Sharma S, Graziotti F, Magenes G (2021) Torsional shear strength of unreinforced brick masonry bed joints. Construct Build Mater 275. https://doi.org/10.1016/j.conbuildmat.2020.122053
Sharma S, Grottoli L, Tomassetti U, Graziotti F (2020) Dataset from shake-table testing of four full-scale URM walls in a two-way bending configuration subjected to combined out-of-plane horizontal and vertical excitation. Data in Brief 31. https://doi.org/10.1016/j.dib.2020.105851
Sharma S, Tomassetti U, Grottoli L, Graziotti F (2020b) Two-way bending experimental response of URM walls subjected to combined horizontal and vertical seismic excitation. Eng Struct 219:1–15
Simsir C, Aschheim M, Abrams D (2004) Out-of-plane dynamic response of unreinforced masonry bearing walls attached to flexible diaphragms. In: 13th World conference on earthquake engineering, pp 1–6
Sorrentino L, D'Ayala D, de Felice G, Griffith M, Lagomarsino S, Magenes G (2017) Review of out-of-plane seismic assessment techniques applied to existing masonry buildings. Int J Archit Herit 11(1):2–21
Sorrentino L, Masiani R, Griffith M (2008) The vertical spanning strip wall as a coupled rocking rigid body assembly. Struct Eng Mech 29(4):433–454
Timoshenko S, Goodier J (1951) Theory of elasticity. McGraw-Hill Education
Tomassetti U, Graziotti F, Penna A, Magenes G (2018) Modelling one-way out-of-plane response of single-leaf and cavity walls. Eng Struct 167:241–255
Vaculik J, Griffith M (2018) Out-of-plane shake table testing of unreinforced masonry walls in two-way bending. Bull Earthq Eng 16(7):2839–2876
Vaculik J, Griffith M (2007) Shaketable tests on masonry walls in two-way bending. In: Australian earthquake engineering society conference
Vaculik J, Griffith M (2017) Out-of-plane load-displacement model for two-way spanning masonry walls. Eng Struct 141:328–343
Vaculik J, Griffith M, Hogarth B, Todd J (2004) Out-of-plane flexural response tests using dry-stack masonry. In: Proceedings of the Australian earthquake society conference. Mt Gambier South Australia
Young W, Plunkett R (2002) Roark's formulas for stress and strain. In: Journal of Applied Mechanics (7th ed.). McGraw-Hill Education. http://appliedmechanics.asmedigitalcollection.asme.org/article.aspx?articleid=1403104